https://doi.org/10.5194/egusphere-2025-966
Preprint. Discussion started: 1 April 2025

Emission characteristics of greenhouse gases and air pollutants in a Qinghai-Tibetan Plateau city using a portable Fourier transform spectrometer and TROPOMI observations

Qiansi Tu[1], Frank Hase[2], Ying Zhang[3], Jiaxin Fang[1], Yanwu Jiang[1], Xiaofan Li[3], Matthias Schneider[2], Zhuolin Yang[3], Xin Zhang[4], Zhengqiang Li[3]

[1]School of Mechanical Engineering, Tongji University, Shanghai 201804, China
[2]Institute of Meteorology and Climate Research (IMK-ASF), Karlsruhe Institute of Technology (KIT), Eggenstein-Leopoldshafen 76344, Germany
[3]State Environmental Protection Key Laboratory of Satellite Remote Sensing, Aerospace Information Research Institute, Chinese Academy of Sciences, Beijing 100101, China
[4]College of Resources and Environment, University of Chinese Academy of Sciences, Beijing 101408, China

Correspondence to: Zhengqiang Li (lizq@radi.ac.cn)

Abstract

Despite the critical need to understand greenhouse gas and air pollutant concentrations and their emissions characteristics in urban and industrial areas, limited assessments have been conducted in the Qinghai-Tibetan Plateau (QTP) cities. Herein, for the first time, we present CO_2, CH_4 and CO column abundances using a portal Fourier-transform infrared spectrometer (EM27/SUN) in Ganhe Industrial Park (36.546°N, 101.518°E, 2603 m a.s.l.), located in the suburbs of Xining, Qinghai Province, during May – June 2024. Ground-based measurements found to be higher than spaceborne measurements (TROPOMI and IASI) and model forecast (CAMS) across all investigated species, indicating higher local emissions. Notably, significant discrepancies in CO levels are observed, particularly under easterly wind conditions, which transport polluted airmasses from Xining city. To further quantify emissions, we applied a simple dispersion model to the EM27/SUN data and TROPOMI products, estimating an average CO emission rate of 12.3 ± 9.6 kg/s and 8.9 ± 7.5 kg/s, respectively. A wind-assigned anomaly method further applied to the TROPOMI dataset yielded a CO emission rate of 8.5 kg/s. Additionally, the ground-based observations of $\Delta XCO/\Delta XCO_2$ ratio exhibits a strong correlation under easterly winds, which suggests an average CO_2 emission rate of 550 kg/s from Xining city. These findings underscore the utility of portable FTIR spectrometers to enhance our understanding of urban emissions at QTP.

1. Introduction

Carbon dioxide (CO_2) and methane (CH_4) are two primary greenhouse gases (GHGs) whose atmospheric concentrations have surged to unprecedented levels since 1750, largely driven by anthropogenic activities. According to the WMO's annual Greenhouse Gas Bulletin (https://library.wmo.int/idurl/4/69057, last access: January, 2024), the globally averaged surface concentration of CO_2 reached 420 parts per million (ppm), and CH_4 reached 1934 parts per billion (ppb) in 2023. Carbon monoxide (CO) is one of the most important atmospheric pollutants, which is primarily produced by inefficient combustion, such as biomass burning (Griffin et al., 2024), traffic and industrial activity (Dils et al., 2011). CO plays a crucial role in atmospheric chemistry, especially in the troposphere, where it reacts with the

https://doi.org/10.5194/egusphere-2025-966
Preprint. Discussion started: 1 April 2025

hydroxyl radical (OH) in the reaction CO + ·OH → CO_2 + ·H (Spivakovsky et al., 2000; Thompson, 1992). This oxidation process serves as the dominant sink for atmospheric CO, accounting for 90-95% of its total removal. Consequently, CO indirectly affects the lifetime of CH_4 by reducing the availability of OH that would otherwise oxidize CH_4. This, in turn, indirectly contributes to global warming (IPCC, 2007).

To achieve highly accurate and precise measurements of total column abundances of CO_2, CH_4 and CO, the Total Carbon Column Observing Network (TCCON) and the Collaborative Carbon Column Observing Network (COCCON) have been established. Both networks utilize Fourier-transform infrared (FTIR) spectrometers. TCCON employs high-resolution FTIR instruments for exceptionally precise CO_2, CH_4 and CO measurements amongst other gases (Wunch et al., 2011). In contrast, COCCON employs portable, low-resolution FTIR spectrometers to measure CO_2, CH_4 and CO, providing a valuable complementary extension to the TCCON network (Alberti et al., 2022; Frey et al., 2015; Herkommer et al., 2024).

The Qinghai-Tibetan Plateau (QTP), with its unique topography, plays a crucial role in Earth's climate system and has become a key region for monitoring climate trends and global air quality (Kang et al., 2021; Zhang et al., 2022). A recent study highlights that surface pollutants in Asia can be transported into the stratosphere from the Tibetan Plateau region, potentially exerting significant impacts on global climate (Bian et al., 2020). There are only two stations on the Tibetan Plateau—Waliguan, the only global station in Eurasia, and Shangri-La—that measure surface concentrations of CO_2, CH_4, and CO, making them important for understanding atmospheric composition in this critical region (Guo et al., 2020; Xiong et al., 2022). These stations conduct in-situ measurements and provide highly accurate surface observations; however, they are influenced by surface exchanges and vertical transport, which can limit their ability to estimate sources and sinks. Additionally, surface observations are less effective for satellite validation compared to column-based measurements, such as those obtained from TCCON and COCCON. However, there are currently no TCCON or COCCON stations on the QTP. Zhou et al. (2023) conducted the first FTIR column observations in a small city on QTP, but measurements in larger cities, such as Xining—the capital of Qinghai Province, remain sparse. This is notable since most anthropogenic emissions of GHGs and CO are concentrated in urban centers (Crippa et al., 2021).

This study presents the EM27/SUN FTIR remote sensing observations conducted in Ganhe Industrial Park (36.546°N, 101.518°E, 2603 m a.s.l.), located in the southwest suburbs of Xining, Qinghai Province during May-June 2024. It includes a comparison to the co-located TROPOMI and IASI observations and CAMS forecasts. Additionally, a simple dispersion model is introduced and applied to estimate the CO and CO_2 emissions.

2. Methods and materials

2.1 Site description

A three-week field campaign was conducted in Ganhe Industrial Park (36.546°N, 101.518°E, 2603 m a.s.l.) from May 23 to June 14, 2024. The industrial park is located southwest of Xining, the capital of Qinghai Province, China (Figure 1) and was established in 2002 in the Huangzhong District. Xining, situated on the eastern edge of the Tibetan Plateau

https://doi.org/10.5194/egusphere-2025-966
Preprint. Discussion started: 1 April 2025

and upstream of the Huangshui River, experiences a plateau mountain climate. In 2020, the city has a resident population of approximately 2.47 million, with a density of 324 persons/km^2 (Xining Statistical Bureau, 2021), making it the most densely populated area in Qinghai Province with nearly 80% of its population living in the urban center.

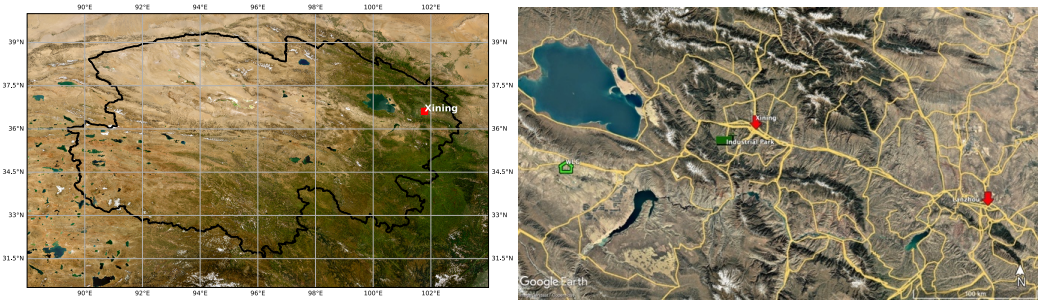

Figure 1: A terrain map showing Qinghai Province and the location of its capital city of Xining (Terrain information originates from World Imagery). A map illustrating the locations of the EM27/SUN instrument within the Ganhe Industrial Park, Xining city (Qinghai province), Lanzhou city (Gansu province), and Waliguan station. The base map is sourced from © Google Earth, Image © 2024 Maxar Technologies; Image © 2024 CNES / Airbus.

2.2 COCCON GHG products

In this study, a portable ground-based Fourier-transform infrared (FTIR) spectrometer, the EM27/SUN, was used. Developed by the Karlsruhe Institute of Technology (KIT) in collaboration with Bruker Optics GmbH, Ettlingen, Germany, the EM27/SUN is designed to measure solar absorption spectra in the near-infrared spectral range (covering 5500–11,000 cm^{-1} and 4000–5500 cm^{-1}) with a spectral resolution of 0.5 cm^{-1} (Gisi et al., 2012). The spectrometer records double-sided, DC-coupled interferograms using two indium gallium arsenide (InGaAs) detectors at room temperature (Hase et al., 2016). These interferograms are processed using a preprocessing tool and the PROFFAST nonlinear least squares fitting algorithm, which was developed by KIT in the framework of the COCCON-PROCEEDS project funded by the European Space Agency (ESA) (Alberti et al., 2022; Herkommer et al., 2024). This approach enables the retrieval of atmospheric concentrations of trace gases such as O_2, CO_2, CH_4, CO and H_2O. The gas column is then converted to column-averaged dry-air mole fractions of the gas (Xgas) by dividing the gas column by the co-observed O_2 column, using the well-known mole fraction of O_2 in dry air.

With meanwhile about 200 EM27/SUN instruments deployed worldwide, these spectrometers are widely used for monitoring GHG concentrations and air pollutant, for estimating emissions from various sources, and for validating satellite measurements (Chen et al., 2020; Frey et al., 2015; Hase et al., 2015; Herkommer et al., 2024; Luther et al., 2019; Tu et al., 2021, 2020). Due to its excellent level of robustness and reliability, the EM27/SUN instrument can be applied in both field campaigns and long-term deployment at fixed sites. These observations complement TCCON at various locations enhances global GHG monitoring efforts. In this context, the COCCON was established to further advance and standardize these observational efforts.

https://doi.org/10.5194/egusphere-2025-966
Preprint. Discussion started: 1 April 2025

2.3 TROPOMI CH_4 and CO products

The TROPOspheric Monitoring Instrument (TROPOMI), single payload of the Sentinel-5 Precursor (S5P) satellite, has been in orbit since October 2017. It operates in a low Earth polar orbit with a planned operational lifespan of 7 years. S5P is the first Copernicus mission and is designed to deliver daily global information on concentrations of traces gases (e.g., CH_4 and CO) and aerosols, aiming to monitor air quality, climate forcing and ozone abundances with high spatial and temporal resolution (Veefkind et al., 2012).

TROPOMI, currently the most advanced nadir-viewing and multispectral imaging spectrometer, was developed jointly by the European Space Agency (ESA) and the Netherlands Space Office. It measures across several spectral bands: ultraviolet (UV) and visible (VIS) (270–500 nm), near-infrared (NIR, 675–775 nm) and shortwave infrared (SWIR, 2305–2385 nm). With a wide swatch of 2600 km across track, TROPOMI provides operational level 2 (L2) CH_4 and CO products with a very high spatial resolution of approximately 5.5 km × 7 km since August 2019.

The retrieval of TROPOMI total column abundances of CH_4 is conducted using the RemoTec-S5P algorithm (Butz et al., 2009; Hasekamp and Butz, 2008). For CO, the total column retrieval is performed by a modified SWIR CO retrieval (SICOR) algorithm, which is based on the CO absorption band between 2305 nm and 2385 nm, with interfering trace gases and effective cloud parameters (Landgraf et al., 2016).

In this study, the TROPOMI L2 CH_4 and CO data with quality assurance values (qa_value) greater than 0.5, as recommend in the S5P product readme files, are utilized. Detailed documentation can be accessed for the CH_4 (https://sentinel.esa.int/documents/247904/3541451/Sentinel-5P-Methane-ProductReadme-File, last accessed: June 9, 2025) and CO data products (https://sentinel.esa.int/documents/247904/3541451/Sentinel-5P-CarbonMonoxide-Level-2-Product-Readme-File, last accessed: June 9, 2025).

2.4 IASI CO products

The Infrared Atmospheric Sounding Interferometer (IASI) is the primary payload carried on the EUMETSAT's MetOp series of polar-orbiting satellites and delivers meteorological parameters (e.g., water vapour and atmospheric temperature), and trace species with an unprecedented spatial and temporal coverage (Clerbaux et al., 2009). IASI sensors are nadir looking thermal infrared sensors and there are currently three instruments in operation, which were launched in 2006, 2012 and 2018.

The IASI CO dataset is processed using the Fast Optimal Retrievals on Layers for IASI (FORLI) software (George et al., 2009; Hurtmans et al., 2012). The retrievals are performed within the 2143-2181.25 cm^{-1} spectral range based on the optimal estimation theory and tabulated absorption cross sections at various pressures and temperatures to enhance the efficiency of the radiative transfer calculation. In this study, total column abundances of CO from IASI onboard Metop-C Level 2 (version 6.7) are used.

https://doi.org/10.5194/egusphere-2025-966
Preprint. Discussion started: 1 April 2025

2.5 CAMS high-resolution GHG forecasts and CAMS-GLOB-ANT inventory

The Copernicus Atmosphere Monitoring Service (CAMS), which is implemented by the European Centre for Medium-Range Weather Forecasts (ECMWF), produces daily global forecasts for the two main long-lived GHGs. As part of the CAMS GHG services, the ECMWF Integrated Forecasting System (IFS) delivers 5-day high-resolution forecasts of CO_2, CH_4 (Agustí-Panareda et al., 2014, 2017, 2019), as well as CO and meteorological parameters essential for GHG forecasting (Flemming et al., 2015). The forecast is generated a few hours behind real time, with initial conditions derived from a 4-day forecast of the analysis experiment. It is run at a horizontal resolution TCo1279, corresponding to a cubic octahedral reduced Gaussian grid with an approximately spatial resolution of 9 km (Holm et al., 2016). The model includes 137 vertical levels extending from the surface to 0.01 hPa (Agustí-Panareda et al., 2019).

In this study, the forecasting suite is based on the IFS model cycle CY48R1, which was upgraded in June 2023. This update introduced several system enhancements, particularly in composition modelling, emissions and assimilation (Eskes et al., 2024). Notably, CY48R1 includes the assimilation of TROPOMI CO and the performance has generally improved compared to all observations, such as surface observations, vertical profiles from IAGOS aircraft and NDACC FTIR measurements, and satellite total column retrievals (Eskes et al., 2024).

CAMS also delivers global anthropogenic emissions, referred to as CAMS-GLOB-ANT. This includes emissions of both air pollutants (e.g., CO) and greenhouse gases (e.g., CO_2 and CH_4) for real-time forecasts (Soulie et al., 2024). Emissions are provided for 17 sectors and 35 species as monthly averages, with a spatial resolution of 0.1° × 0.1°, covering the period from 2000 to 2025. This study uses the latest version v6.2, which is based on the Emissions Database for Global Atmospheric Research (EDGARv6) and employs the same methodology as v5.3.

3. Results and discussion

3.1 Ground-based observations

Figure 2 illustrates the time-series of XCO_2, XCH_4 and XCO observed by the EM27/SUN over 8 intermittent days. Among these gases, XCO exhibits the most significant intraday variability, particularly on May 25, 27 and June 14. During these days, prevailing easterly winds transported airmasses from Xining City and the nearby highway (Xiong et al., 2022), leading to the elevated XCO levels. In contrast, on June 4, when airmasses primarily originated from the west and northwest—regions with less urbanized areas—XCO levels were notably stable and low, averaging 93.93 ± 4.23 ppb (see back trajectories on Figure A 2). Additionally, higher wind speed on June 4 facilitated the dispersion of CO, contributing to the lower CO level.

Similarly, XCO_2 on June 4 showed relatively less intraday variability and a lower average concentration of 424.64 ± 0.25 ppm, except for a slight enhancement (~1 ppm) in the morning, which was also observed in XCH_4 (~6 ppb). This suggests different CO sources in the western areas relative to the EM27/SUN location.

https://doi.org/10.5194/egusphere-2025-966
Preprint. Discussion started: 1 April 2025

The observed average XCH_4 concentration during the measurement period was 1899.947 ± 7.04 ppb. This relatively low variability suggests an absence of significant local methane sources, such as coal mining activities (Tu et al., 2024a), which are known to emit substantial amounts of methane.

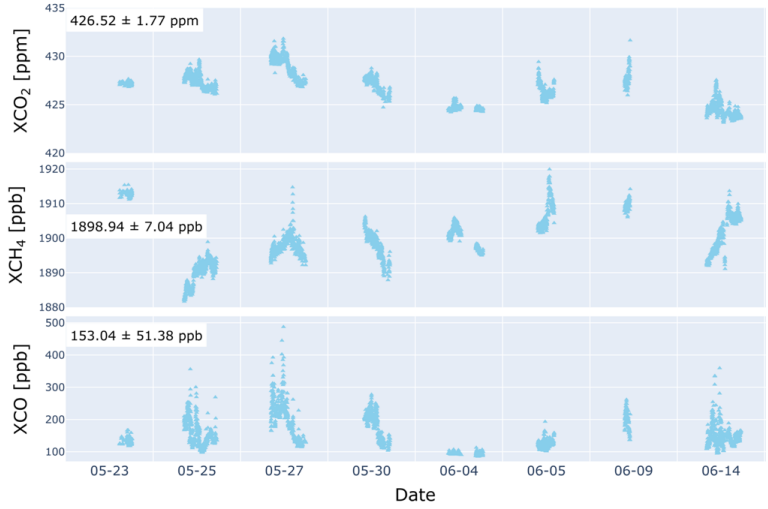

Figure 2: time-series of EM27/SUN observations from May 23 to June 14 2024.

3.2 Comparison of COCCON data with TROPOMI and IASI products

Figure 3a-b illustrates the correlations between TROPOMI and COCCON measurements on different days. The spatial collocation criterion requires the TROPOMI observations to fall within a radius of 200 km for XCH_4 and 100 km for XCO. The temporal collocation criterion is set to ±2h for COCCON measurements.

The results indicate that TROPOMI tends to slightly overestimate XCH_4 by an average bias of -2.84 ± 12.74 ppb, while it significantly underestimates of XCO, showing a bias of 34.31 ± 24.45 ppb. The correlation between TROPOMI and COCCON XCH_4 measurements improves as the spatial distance between their respective locations decreases. The largest observed difference in XCH_4, approximately -20.66 ppb, occurs on June 14, when the minimal distance between TROPOMI and COCCON locations is around 150 km (Figure A 3a).

A similar trend is observed for XCO, where larger biases are generally associated with greater distances. However, on May 27, the largest bias (69.23 ppb) occurs despite a relatively small minimum distance of 13 km. This significant discrepancy is likely influenced by the spatial distribution of TROPOMI observations relative to the EM27/SUN location. Notably, on May 27, TROPOMI XCO levels exhibit a negative correlation with distance for observations within approximately 100 km (Figure A 3b). The closest observation to the EM7/SUN location records a TROPOMI XCO value of 157.20 ppb, resulting in a significantly reduced bias of 16.72 ppb.

For May 23, four TROPOMI XCO observations, with distances ranging from 2.8 km to 10.4 km, result in a mean value of 132.43 ppb. These closer observations show an overestimation in XCO, with a difference of 8 ppb compared

https://doi.org/10.5194/egusphere-2025-966
Preprint. Discussion started: 1 April 2025

to the EM27/SUN measurements. However, this discrepancy could be influenced by the fact that EM27/SUN observations were available only one hour after the TROPOMI overpass, potentially introducing temporal variations into the comparison.

The correlation between IASI and COCCON is relatively higher (R^2 = 0.6478) compared to the correlation between TROPOMI and COCCON XCO. Similar to TROPOMI, IASI shows the highest bias on May 27 with a value of 2.43E22 molec./m^2. Enhanced CO levels are observed within 20 km radius, with the peak CO concentration reaching 2.66E22 molec./m^2 at 15.4 km (Figure A 3c). As a result, the bias decreases by nearly half to 1.32E22 molec./m^2.

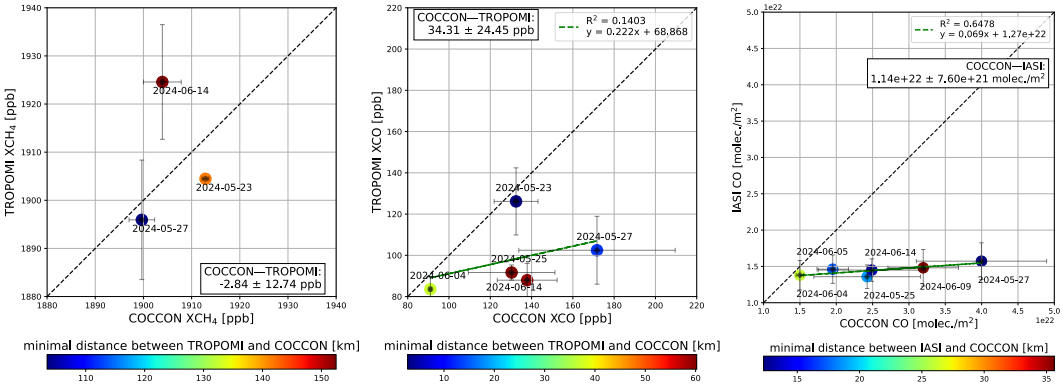

Figure 3: Correlation plot between TROPOMI and COCCON for XCH4 (a) and XCO (b) and between IASI and COCCON for CO column (c). The color bar represents the minimum distance between the TROPOMI and COCCON locations.

3.3 Comparison of COCCON data with CAMS products

The CAMS GHG forecast provides a high spatial resolution of approximately 9 km. For comparison with the EM27/SUN site, the following coincidence criteria were used: CAMS data within a 20 km radius of the EM27/SUN location and EM27/SUN observations within ± 2h around noon.

The CAMS forecast XCH_4 demonstrates a strong correlation (R^2 = 0.7930) with COCCON observations and an average bias of 4.86 ± 3.81 ppb. The mean bias increases to 8.87 ppb when a larger coincidence radius of 50 km is used for the CAMS dataset. The correlation slightly decreases, with the R^2 value dropping to 0.7877.

CAMS generally underestimates XCO_2 and the CO column, exhibiting lower correlations. The mean biases are 1.66 ± 1.50 ppm for XCO_2 and 1.01E22 ± 6.31E21 molec./m^2 for CO. The largest biases in XCO_2 and CO are recorded on May 27. This discrepancy is also observed in TROPOMI and IASI CO observations.

https://doi.org/10.5194/egusphere-2025-966
Preprint. Discussion started: 1 April 2025

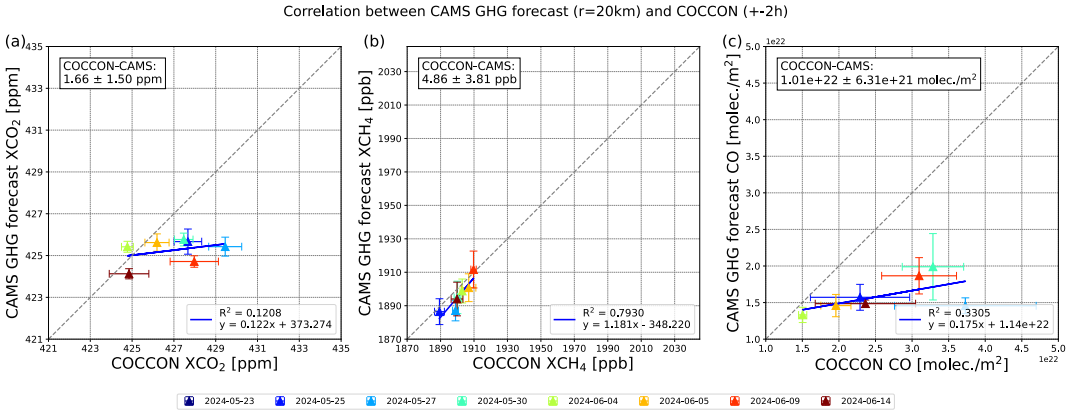

Figure 4: Correlation between CAMS forecast and COCCON for XCO_2 (a), XCH_4 (b) and CO column (c).

3.4 CO emission estimates based on ground-based observations

Satellite observations, such as TROPOMI and IASI, and CAMS forecasts, consistently underestimate CO levels during the entire field campaign. Thus, ground-based measurements are essential for accurately estimating CO emissions. Wind directions predominantly originated from the east (Figure A 1) on five days, indicating that emissions from the Xining city were being transported to the downwind site where the EM27/SUN located.

Figure 5 highlights the correlation between ΔXCO multiplied by wind speed as a function of wind direction. Wind directions within the range of 80° – 120°, associated with relatively higher multiplication between ΔXCO and wind speed, were selected to represent the predominant winds transporting emissions from Xining. In this range, the average wind speed is approximately 2.3 m/s, with a standard deviation of 0.7 m/s. To account for variability, an uncertainty of ±20º is applied. The wind spreading angle ∂ is defined as:

$$\partial = 120° - 80° = 40°(\pm 20°) = 0.7\ (\pm 0.35)\ rad$$

Based on this wind spreading angle, the CO emission is calculated using the dispersion model as shown in the following equation (Babenhauserheide et al., 2020; Tu et al., 2022a):

$$\varepsilon = \Delta\mathrm{CO} \times d \times v \times \partial \qquad \textbf{Eq. 1}$$

where ΔCO represents the enhanced CO column observed at the EM27/SUN site, d is the average distance from Xining city to the EM27/SUN location (approximately 25 km) and v is the wind speed.

https://doi.org/10.5194/egusphere-2025-966
Preprint. Discussion started: 1 April 2025

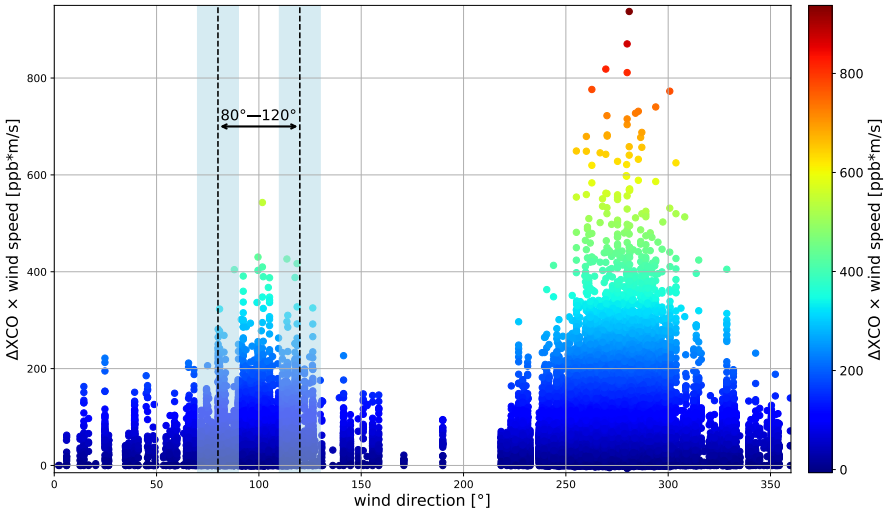

Figure 5: TROPOMI ΔXCO multiplied by wind speed against the wind direction for wind speed greater than 1.5 m/s, covering the period from May 2018 to June 2024. Wind data are derived from ERA5 at a heigh of 100m above ground level at the EM27/SUN station at 14:00 local time. The ΔXCO dataset represents XCO residuals after background subtraction. The wind direction range of 80°–120° (delineated by dashed lines) captures the predominant wind influence from Xining city. The shaded areas represent the uncertainty of 10°.

The daily background concentration of CO is defined as the lowest 10th percentile of measurements. To minimize accidental bias, a 10-minuten averaged EM27/SUN CO dataset was used. Significant enhancements are observed in ΔXCO and ΔXCO_2 in the 80°-120° wind direction range (Figure A 4). Using Equation (2), the estimated CO emissions for five days are presented in Figure 6. Notably, relatively high emissions were observed in the 80°-120° wind direction range, corresponding to areas of higher wind speed. A similar enhancement of CO associated with easterly winds was reported by Xiong et al. (2022), where in situ observations at the Waliguan station (36.28°N, 100.09°E, 3816 m a.s.l.), located approximately 155 km southwest of Xining city. This highlights the influence of regional air transport on the observed CO concentrations.

The CO emissions in the wind direction interval of 80°-120° are likely attributed to Xining city, with a mean estimated emission rate of 2.7E26 ± 2.1E26 molec./s (i.e., 12.3 ± 9.6 kg/s). The maximum emission rate reached 1.2E27 molec./s (i.e., 55.6 kg/s) on May 27, a day when both satellite observations and forecasts underestimated the CO levels. The peak emission on May 27 occurred around noon, coinciding with a significant enhancement in XCO, which reached an approximate 10-minute averaged signal of 300 ppb.

Another notable high emission event was observed on May 25 and 30, under wind directions around 60°. These elevated emissions are likely to attributed to emission from the north-northeast region of the EM27/SUN location. On May 25, an enhanced XCO signal (~80 ppb) was observed in the late afternoon, coinciding with a relatively higher wind speed of ~2.8 m/s, which contributed to the increased emissions. On March 30, the XCO signal peaked at ~120 ppb around noon, leading to even higher emission rates.

https://doi.org/10.5194/egusphere-2025-966
Preprint. Discussion started: 1 April 2025

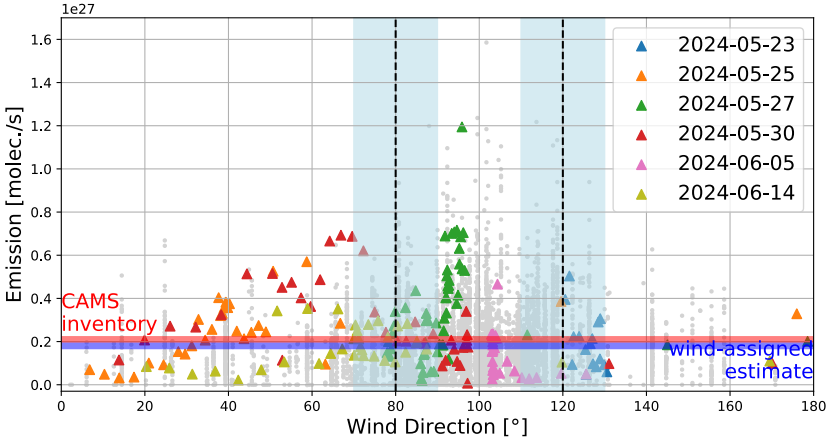

Figure 6: Estimated emission relative to wind direction on six days of ground-based measurements (triangle symbols) when winds were predominantly easterly. Grey dots represent emissions derived from TROPOMI XCO. Two horizontal lines indicate CO emission rates derived from the wind-assigned anomaly method and the CAMS-GLOB-ANT inventory, respectively.

3.5 CO emission estimates based on satellite-based observations

TROPOMI observes relative high CO levels near the central region of Xining. A distinct streak of elevated CO concentrations extends eastward from Xining toward the Qinghai province border and continues toward Lanzhou in Gansu province (not shown in the figure). This pattern aligns with the location of densely populated residential regions and coincides with a gradual decrease in altitude from west to east (Figure A 5).

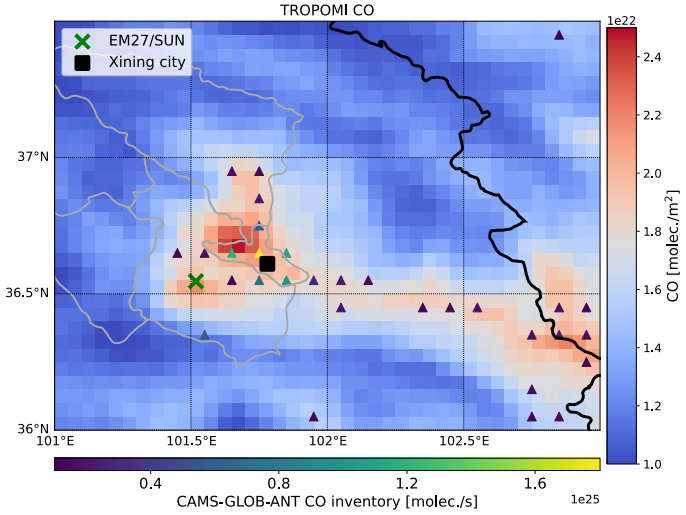

Figure 7: Spatial distribution of the average TROPOMI CO column at a latitude-longitude resolution of 0.05°, covering the period from May 2018 to June 2024. The triangle symbols indicate locations where CO emissions exceed 1E24 molec./s based on the CAMS-GLOB-ANT inventory. The green cross marks the location of the EM27/SUN and the black square

https://doi.org/10.5194/egusphere-2025-966
Preprint. Discussion started: 1 April 2025

represents the center of Xining city. The thick black line outlines the Qinghai province boundary and the thin grey lines delineate subregions within Xining.

Emissions derived from TROPOMI CO products, based on the Eq1. are presented in Figure 6 (grey dots), showing relatively higher values for wind directions between 80º and 120º. The average emission rate is approximately 8.9 ± 7.5 kg/s, which closely matches the emissions derived from the COCCON measurements.

To further estimate regional CO emissions, a wind-assigned method in combination with the dispersion model described in Eq.1 is applied to the TROPOMI observations. The wind-assigned method, previously used for estimating regional CH_4 and NO_2 emissions (Tu et al., 2024b, 2023, 2022a, 2022b), by fitting the wind-assigned anomalies between the satellite observations and the modeled anomaly based on the dispersion model. The wind-assigned anomaly is defined as the difference in the enhancements under two opposite wind fields, e.g., E (>0º and <180º) and W (180º-360º) fields. This approach eliminates the uncertainty associated with calculating the background for long-lifetime gases (e.g., for CH_4), thus improving the reliability of emission estimates.

The estimated CO emission based on the wind-assigned anomaly method is approximately 1.8E26 molec./s (8.5 kg/s), which is close to the CAMS-GLOB-ANT inventory (2.1E26 molec./s, i.e., 9.8 kg/s) and the average emission derived from the six-day EM27/SUN measurements (2.7E26 molec./s, i.e., 12.3 kg/s). However, scatters are observed in the correlation between the TROPOMI and modeled wind-assigned anomalies, leading to a lower R^2 value (Figure 8). This discrepancy could originate from uncertainties in the CAMS inventory, which may not account for some some-high emission sources. Additionally, the simple dispersion model introduces its own uncertainties, which limits the ability to accurately model CO enhancements.

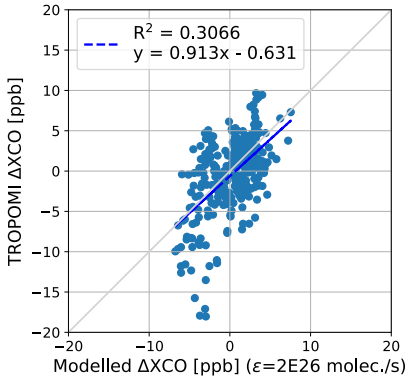

Figure 8: Correlation in the wind-assigned anomalies between the TROPOMI observations and modeled anomalies.

3.6 CO_2 estimates based on combustion efficiency

In urban environments, CO is primarily produced through the incomplete combustion of fossil fuels, such as those from traffic emissions and industrial activities, often occurring alongside the formation of CO_2. The CO to CO_2 ratio serves as a valuable indicator for atmospheric fossil-fuel CO_2 emissions and combustion efficiency, providing insights into the sources and effectiveness of fuel use (Che et al., 2022; Lee et al., 2024; Sim et al., 2020).

https://doi.org/10.5194/egusphere-2025-966
Preprint. Discussion started: 1 April 2025

Figure 9 presents the relationship between ΔXCO and ΔXCO_2 under predominant wind of wind direction of 80° – 120° and wind speed larger than 1.5 m/s for different days. The daily background concentrations of XCO_2 and XCO were determined as the lowest 10th percentile of the respective observations. ΔXCO and ΔXCO_2 was calculated by subtracting the daily background concentrations from the daily observed values. Under easterly wind conditions, ΔXCO exhibits a stronger correlation with ΔXCO_2, with a slope of 35.14 (ppb/ppm) and an R^2 value of 0.7552, indicating distinct source contributions and atmospheric transport processes from eastern regions, such as Xining city. The observed $\Delta XCO/\Delta XCO_2$ ratio is higher than those reported in other studies (Che et al., 2022; Lee et al., 2024). This discrepancy is attributed to significantly elevated CO levels under easterly wind conditions, suggesting lower combustion efficiency in this region.

Using CO as a proxy, the fossil fuel-derived CO_2 emissions can be computed as follows:

$$E_{CO_2} = \left(\frac{1}{ER_{CO/CO_2}} \times \frac{M_{CO_2}}{M_{CO}}\right) E_{CO} \qquad \textbf{Eq. 2}$$

Where E_{CO_2} is the emissions of CO_2 in kg/s, ER_{CO/CO_2} is the ratio of $\Delta XCO:\Delta XCO_2$ in ppb/ppm, E_{CO} is the CO emission rate derived based on Sec. 3.4, and M_{CO_2} and M_{CO} are the molar mass of CO_2 and CO, respectively.

We estimate an average CO_2 emission rate of approximately 550 kg/s. The maximum $\Delta XCO:\Delta XCO_2$ ratio was observed on May 27, with a slope of 40.08 (R^2 = 0.8544), corresponding to a maximum CO emission rate of 55.6 kg/s and resulting in a maximum CO_2 emission rate of 2180 kg/s. This estimate aligns reasonably with the Carbon Emission Accounts and Datasets (CEADs) inventory, with reports a CO_2 emission rate of 726 kg/s for Xining in 2015 ("Methodology and applications of city level CO2 emission accounts in China," 2017; Shan et al., 2018). The observed discrepancies may be attributed to differences in temporal coverage, methodological approaches, and potential changes in emission patterns over time. A longer period of ground-based observations and running several spectrometers upwind and downwind may improve our results. Our findings so far demonstrate the potential of the EM27/SUN spectrometer as a promising tool for comprehensively evaluating greenhouse gas (GHG) and air pollutant emissions in urban areas (Che et al., 2022; Lee et al., 2024).

https://doi.org/10.5194/egusphere-2025-966
Preprint. Discussion started: 1 April 2025

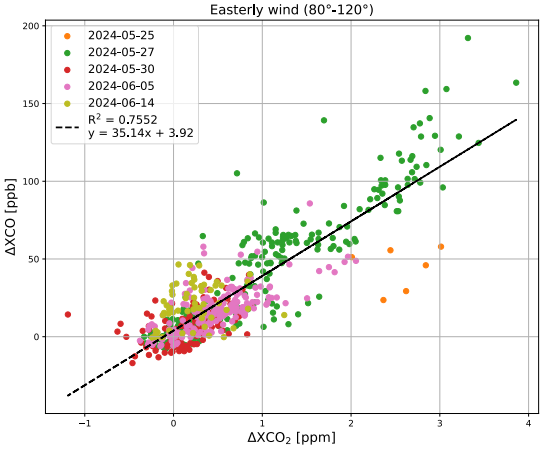

Figure 9: ΔXCO/ΔXCO₂ ratios under easterly wind conditions covering direction between 80° and 120°. Different colors indicate observations from individual days.

Conclusion

A three-week field campaign using a portal FTIR spectrometer (EM27/SUN) was conducted at Ganhe Industrial Park, located in the southwestern suburbs of Xining city, from May 23 to June 14, 2024. The mean and standard deviation values for XCO_2, XCH_4 and XCO were 426.52±1.77 ppm, 1898.94±7.04 ppb and 153.04±51.38 ppb, respectively. Among these gases, XCO exhibited significant intraday variability, particularly on days dominated by easterly winds, which transported airmass from Xining city.

Ground-based observations were compared with co-located datasets from TROPOMI, IASI and CAMS. Results indicate that TROPOMI slightly overestimates XCH_4, with an average bias of -2.84 ± 12.74 ppb, but significantly underestimates XCO, showing a bias of 34.31 ± 24.45 ppb. IASI generally underestimates the CO column relative to COCCON observations, with an average bias of 1.14E22 ± 7.60E21 molec./m^2. CAMS forecasts also underestimated XCO_2 (1.66 ± 1.50 ppm), XCH_4 (4.86± 3.81 ppb) and CO column (1.01E22 ± 6.31E21 molec./m^2). A high correlation (R^2=0.7930) was found for XCH_4 between CAMS and EM27/SUN datasets. The largest discrepancies in CO products occurred on May 27, when significant enhancements were observed at the co-located time by EM27/SUN. These discrepancies are partly attributed to satellite observations, as their concentrations decreased with distance from the EM27/SUN location.

Wind directions predominantly originated from the east on five measurement days, indicating that emissions from the Xining city were being transported to the downwind site where the EM27/SUN spectrometer was located. A simple dispersion model, incorporating wind information and enhanced CO column data from EM27/SUN instrument, was applied to estimate CO emissions. The CO emissions from Xining city are estimated at 12.3 ± 9.6 kg/s with a peak emission rate of 55.6 kg/s on May 27, when both satellite observations and forecasts underestimated CO levels. When this model was applied to TROPOMI CO data, the resulting average emission rate was 8.9 ± 7.5 kg/s. A wind-assigned

https://doi.org/10.5194/egusphere-2025-966
Preprint. Discussion started: 1 April 2025

anomaly method was also applied to the TROPOMI CO dataset, resulting in an estimate emission rate of 8.5 kg/s. Both EM27/SUN-based and TROPOMI-based estimates are comparable to the CAMS inventory value of 9.8 kg/s.

CO can serve as a proxy for fossil fuel-derived CO_2 emissions. Ground-based obversions of ΔXCO and ΔXCO_2 exhibit a stronger correlation under wind direction of 80°– 120°, with a slope of 35.14 ppb/ppm and an R^2 value of 0.7552, compared to conditions under westerly winds. Using these correlations, we estimated the CO_2 emission rate to have an average value of 550 kg/s with a maximum value of 2180 kg/s. These estimates align reasonably with the CEASs inventory, which reports a CO_2 emission rate of 726kg/s for Xining in 2015. Observed discrepancies may be attributed to differences in temporal coverage, methodological approaches, and potential changes in emission patterns over time. Note that long-term ground-based measurements of trace gases may improve the precision of estimated emissions.

Our findings highlight the potential of the EM27/SUN spectrometer as a valuable tool for detecting local emission and supporting satellite validation, particularly in high-altitude regions such as Tibetan Plateau. It also demonstrates the ability to efficiently measure both GHG and air pollutant emissions, offering a cost-efficient approach.

https://doi.org/10.5194/egusphere-2025-966
Preprint. Discussion started: 1 April 2025

Data availability.

The TROPOMI CH4 and CO dataset is a Copernicus operational product and is available at https://doi.org/10.5270/S5P-3lcdqiv (Copernicus Sentinel-5P, 2021). The access and use of any Copernicus Sentinel data available through the Copernicus Open Access Hub are governed by the legal notice on the use of Copernicus Sentinel Data and Service Information, which is given at https://sentinels.copernicus.eu/documents/247904/690755/Sentinel_Data_Legal_Notice (last access: January 2025). IASI CO dataset is available at https://iasi.aeris-data.fr/co/ (last access: January 2025). CAMS forecasts are available at 10.24381/93910310 (last access: January 2025) and CAMS-GLOB-ANT inventory data are available at https://doi.org/10.24380/eets-qd81 (last access: January 2025). CEADS inventory is available at: https://www.ceads.net/data/city?#1280. last access: January 2024.

Author contributions.

QT and FH conceived the research question. QT wrote the manuscript and conducted the data analysis with input from FH. XL and ZY carried out the measurements, while YJ and JF was responsible for the data processing. All authors contributed to the interpretation of the results and the improvement of the paper.

Declaration of Competing Interest.

The authors declare that they have no known competing financial interests or personal relationships that could have appeared to influence the work reported in this paper.

Acknowledgements.

We would like to thank Copernicus User Support Team at ECMWF for providing the CAMS model data. We thank the TROPOMI team for making CH4 and CO data and IASI team for CO data publicly available.

Financial support.

This research was funded by the National Natural Science Foundation of China (grant no. 42305138) and the National Key Research and Development Program (2022YFE0209500).

https://doi.org/10.5194/egusphere-2025-966
Preprint. Discussion started: 1 April 2025

Appendix

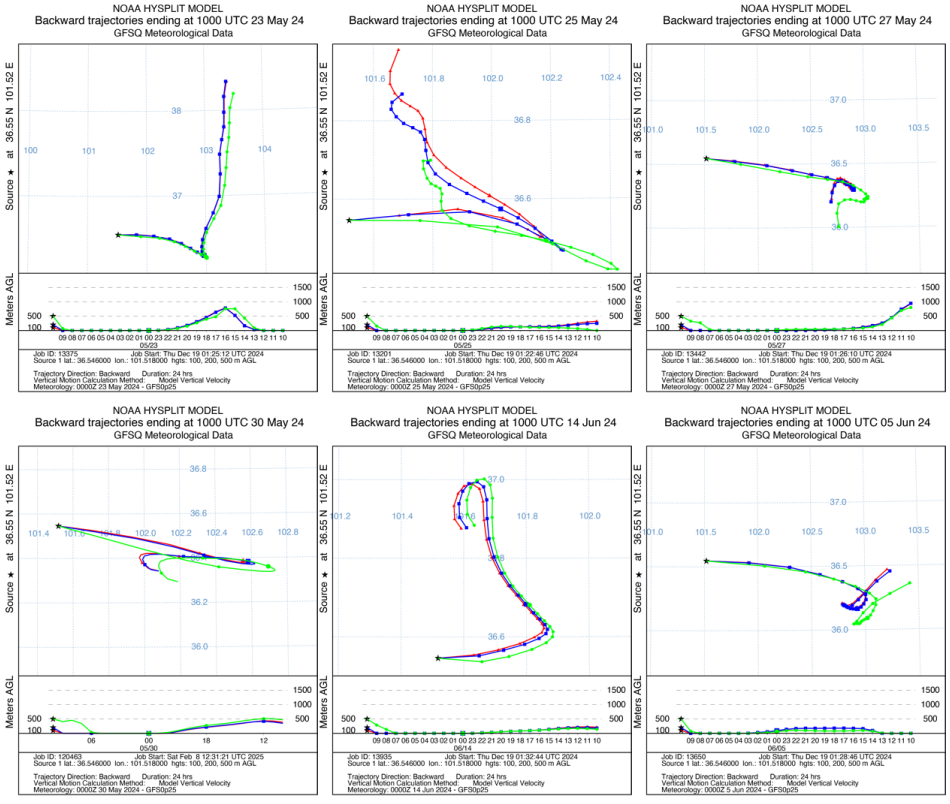

Figure A 1 The back trajectories originating from eastern areas and arriving at EM27/SUN station at 10 UTC (18 Local time) on different days. The trajectories, calculated using the HYSPLIT model (Hybrid Single-Particle Lagrangian Integrated Trajectory), and shown for height of 100, 200 and 500 m above ground level.

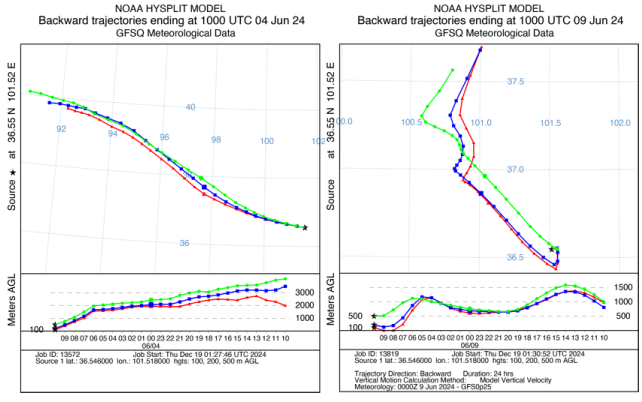

Figure A 2 Similar to Figure A 1, but for trajectories generally from western areas on June 4 and 9, 2024.

https://doi.org/10.5194/egusphere-2025-966
Preprint. Discussion started: 1 April 2025

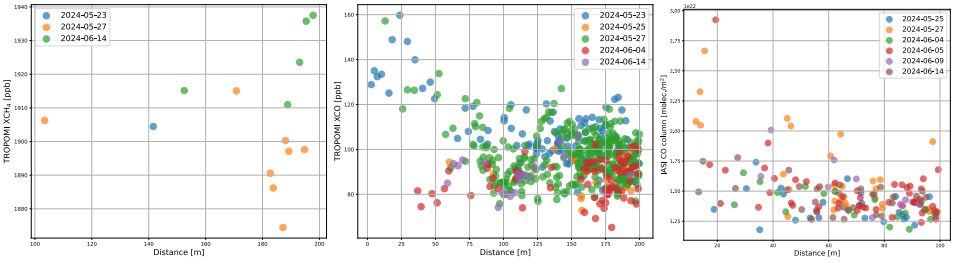

374

375 **Figure A 3: Correlation between TROPOMI XCH_4 (a) and XCO (b) with the distance from each TROPOMI observation**
376 **to the EM27/SUN location. Panel (c) shows the correlation between IASI CO and the distance from each IASI observation**
377 **to the EM27/SUN location.**

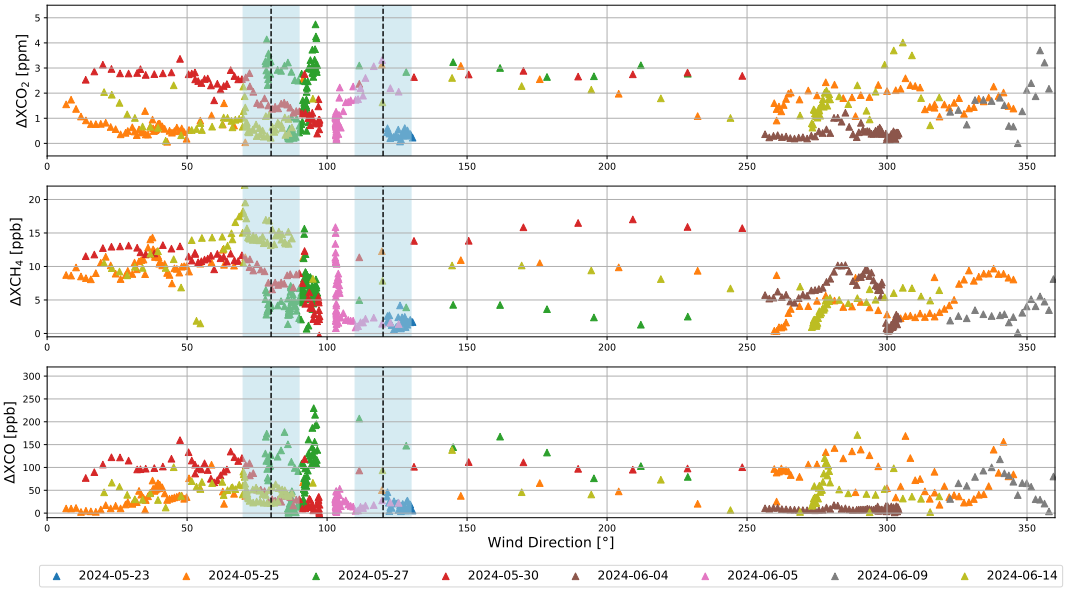

378

379 **Figure A 4: correlations between ΔXCO_2, ΔXCH_4 and ΔXCO with wind direction. The wind direction range of 80°-120° is**
380 **delineated by dashed lines.**

https://doi.org/10.5194/egusphere-2025-966
Preprint. Discussion started: 1 April 2025

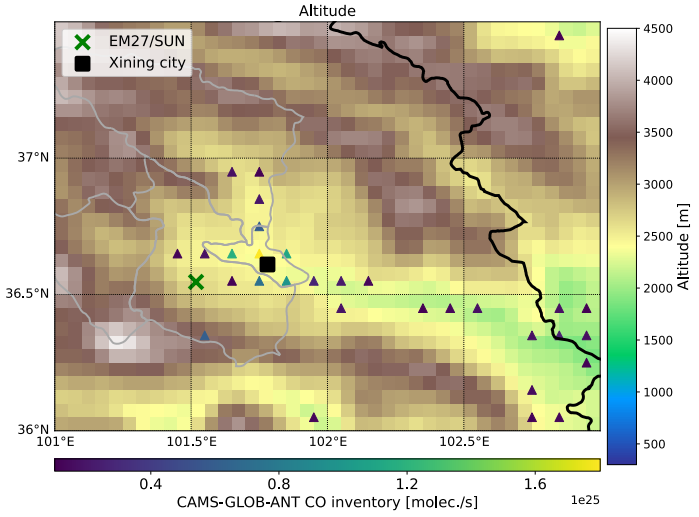

Figure A 5: similar to Figure 7 but for terrain distribution.

https://doi.org/10.5194/egusphere-2025-966
Preprint. Discussion started: 1 April 2025

Reference

Holm, E., Forbes, R., Lang, S., Magnusson, L., and Malardel, S.: New model cycle brings higher resolution, ECMWF Newsletter, ECMWF, Reading UK, No. 147, available at: https://www.ecmwf.int/en/elibrary/16299-newsletter-no-147-spring-2016 (last access: Januray 2024), 2016.

Xining Statistical Bureau. Xining statistical yearbook. 2001. 2021-11-26. https://tjj.xining.gov.cn/zwgk/fdzdgknr/tjxx/gjnj/202111/t20211126_159614.html.

IPCC. (2007). In S. Solomon, D. Qin, M. Manning, Z. Chen, M. Marquis, K. B. Averyt, et al. (Eds.), Climate Change 2007: The Physical Science Basis. Contribution of Working Group I to the Fourth Assessment Report of the International Panel on Climate Change (p. 996). Cambridge University Press.

Carbon Emission Accounts and Datasets (CEADs), 2018. The Emission Inventories for 290 Chinese Cities from 1997 to 2019. available at: https://www.ceads.net/data/city?#1280. last access: January 2024.

Agusti-Panareda, A., Diamantakis, M., Bayona, V., Klappenbach, F., Butz, A., 2017. Improving the inter-hemispheric gradient of total column atmospheric CO_2 and CH_4 in simulations with the ECMWF semi-Lagrangian atmospheric global model. Geoscientific Model Development 10, 1–18. https://doi.org/10.5194/gmd-10-1-2017

Agustí-Panareda, A., Diamantakis, M., Massart, S., Chevallier, F., Muñoz-Sabater, J., Barré, J., Curcoll, R., Engelen, R., Langerock, B., Law, R.M., Loh, Z., Morguí, J.A., Parrington, M., Peuch, V.-H., Ramonet, M., Roehl, C., Vermeulen, A.T., Warneke, T., Wunch, D., 2019. Modelling CO_2 weather – why horizontal resolution matters. Atmospheric Chemistry and Physics 19, 7347–7376. https://doi.org/10.5194/acp-19-7347-2019

Agustí-Panareda, A., Massart, S., Chevallier, F., Boussetta, S., Balsamo, G., Beljaars, A., Ciais, P., Deutscher, N.M., Engelen, R., Jones, L., Kivi, R., Paris, J.-D., Peuch, V.-H., Sherlock, V., Vermeulen, A.T., Wennberg, P.O., Wunch, D., 2014. Forecasting global atmospheric CO_2. Atmospheric Chemistry and Physics 14, 11959–11983. https://doi.org/10.5194/acp-14-11959-2014

Alberti, C., Hase, F., Frey, M., Dubravica, D., Blumenstock, T., Dehn, A., Castracane, P., Surawicz, G., Harig, R., Baier, B.C., Bès, C., Bi, J., Boesch, H., Butz, A., Cai, Z., Chen, J., Crowell, S.M., Deutscher, N.M., Ene, D., Franklin, J.E., García, O., Griffith, D., Grouiez, B., Grutter, M., Hamdouni, A., Houweling, S., Humpage, N., Jacobs, N., Jeong, S., Joly, L., Jones, N.B., Jouglet, D., Kivi, R., Kleinschek, R., Lopez, M., Medeiros, D.J., Morino, I., Mostafavipak, N., Müller, A., Ohyama, H., Palmer, P.I., Pathakoti, M., Pollard, D.F., Raffalski, U., Ramonet, M., Ramsay, R., Sha, M.K., Shiomi, K., Simpson, W., Stremme, W., Sun, Y., Tanimoto, H., Té, Y., Tsidu, G.M., Velazco, V.A., Vogel, F., Watanabe, M., Wei, C., Wunch, D., Yamasoe, M., Zhang, L., Orphal, J., 2022. Improved calibration procedures for the EM27/SUN spectrometers of the COllaborative Carbon Column Observing Network (COCCON). Atmospheric Measurement Techniques 15, 2433–2463. https://doi.org/10.5194/amt-15-2433-2022

https://doi.org/10.5194/egusphere-2025-966
Preprint. Discussion started: 1 April 2025

417 Babenhauserheide, A., Hase, F., Morino, I., 2020. Net CO_2 fossil fuel emissions of Tokyo estimated directly from
418 measurements of the Tsukuba TCCON site and radiosondes. Atmospheric Measurement Techniques 13,
419 2697–2710. https://doi.org/10.5194/amt-13-2697-2020

420 Bian, J., Li, D., Bai, Z., Li, Q., Lyu, D., Zhou, X., 2020. Transport of Asian surface pollutants to the global stratosphere
421 from the Tibetan Plateau region during the Asian summer monsoon. National Science Review 7, 516–533.
422 https://doi.org/10.1093/nsr/nwaa005

423 Butz, A., Hasekamp, O.P., Frankenberg, C., Aben, I., 2009. Retrievals of atmospheric CO_2 from simulated space-
424 borne measurements of backscattered near-infrared sunlight: accounting for aerosol effects. Appl. Opt., AO
425 48, 3322–3336. https://doi.org/10.1364/AO.48.003322

426 Che, K., Liu, Y., Cai, Z., Yang, D., Wang, H., Ji, D., Yang, Y., Wang, P., 2022. Characterization of Regional
427 Combustion Efficiency using ΔXCO: ΔXCO2 Observed by a Portable Fourier-Transform Spectrometer at an
428 Urban Site in Beijing. Adv. Atmos. Sci. 39, 1299–1315. https://doi.org/10.1007/s00376-022-1247-7

429 Chen, J., Dietrich, F., Maazallahi, H., Forstmaier, A., Winkler, D., Hofmann, M.E.G., Denier van der Gon, H.,
430 Röckmann, T., 2020. Methane emissions from the Munich Oktoberfest. Atmospheric Chemistry and Physics
431 20, 3683–3696. https://doi.org/10.5194/acp-20-3683-2020

432 Clerbaux, C., Boynard, A., Clarisse, L., George, M., Hadji-Lazaro, J., Herbin, H., Hurtmans, D., Pommier, M., Razavi,
433 A., Turquety, S., Wespes, C., Coheur, P.-F., 2009. Monitoring of atmospheric composition using the thermal
434 infrared IASI/MetOp sounder. Atmospheric Chemistry and Physics 9, 6041–6054.
435 https://doi.org/10.5194/acp-9-6041-2009

436 Crippa, M., Guizzardi, D., Pisoni, E., Solazzo, E., Guion, A., Muntean, M., Florczyk, A., Schiavina, M., Melchiorri,
437 M., Hutfilter, A.F., 2021. Global anthropogenic emissions in urban areas: patterns, trends, and challenges.
438 Environ. Res. Lett. 16, 074033. https://doi.org/10.1088/1748-9326/ac00e2

439 Dils, B., Cui, J., Henne, S., Mahieu, E., Steinbacher, M., De Mazière, M., 2011. 1997–2007 CO trend at the high
440 Alpine site Jungfraujoch: a comparison between NDIR surface in situ and FTIR remote sensing observations.
441 Atmospheric Chemistry and Physics 11, 6735–6748. https://doi.org/10.5194/acp-11-6735-2011

442 Eskes, H., Tsikerdekis, A., Ades, M., Alexe, M., Benedictow, A.C., Bennouna, Y., Blake, L., Bouarar, I., Chabrillat,
443 S., Engelen, R., Errera, Q., Flemming, J., Garrigues, S., Griesfeller, J., Huijnen, V., Ilić, L., Inness, A.,
444 Kapsomenakis, J., Kipling, Z., Langerock, B., Mortier, A., Parrington, M., Pison, I., Pitkänen, M., Remy, S.,
445 Richter, A., Schoenhardt, A., Schulz, M., Thouret, V., Warneke, T., Zerefos, C., Peuch, V.-H., 2024.
446 Technical note: Evaluation of the Copernicus Atmosphere Monitoring Service Cy48R1 upgrade of June 2023.
447 Atmospheric Chemistry and Physics 24, 9475–9514. https://doi.org/10.5194/acp-24-9475-2024

448 Flemming, J., Huijnen, V., Arteta, J., Bechtold, P., Beljaars, A., Blechschmidt, A.-M., Diamantakis, M., Engelen, R.J.,
449 Gaudel, A., Inness, A., Jones, L., Josse, B., Katragkou, E., Marecal, V., Peuch, V.-H., Richter, A., Schultz,

https://doi.org/10.5194/egusphere-2025-966
Preprint. Discussion started: 1 April 2025

M.G., Stein, O., Tsikerdekis, A., 2015. Tropospheric chemistry in the Integrated Forecasting System of ECMWF. Geoscientific Model Development 8, 975–1003. https://doi.org/10.5194/gmd-8-975-2015

Frey, M., Hase, F., Blumenstock, T., Groß, J., Kiel, M., Mengistu Tsidu, G., Schäfer, K., Sha, M.K., Orphal, J., 2015. Calibration and instrumental line shape characterization of a set of portable FTIR spectrometers for detecting greenhouse gas emissions. Atmos. Meas. Tech. 8, 3047–3057. https://doi.org/10.5194/amt-8-3047-2015

George, M., Clerbaux, C., Hurtmans, D., Turquety, S., Coheur, P.-F., Pommier, M., Hadji-Lazaro, J., Edwards, D.P., Worden, H., Luo, M., Rinsland, C., McMillan, W., 2009. Carbon monoxide distributions from the IASI/METOP mission: evaluation with other space-borne remote sensors. Atmospheric Chemistry and Physics 9, 8317–8330. https://doi.org/10.5194/acp-9-8317-2009

Gisi, M., Hase, F., Dohe, S., Blumenstock, T., Simon, A., Keens, A., 2012. XCO2-measurements with a tabletop FTS using solar absorption spectroscopy. Atmos. Meas. Tech. 5, 2969–2980. https://doi.org/10.5194/amt-5-2969-2012

Griffin, D., Chen, J., Anderson, K., Makar, P., McLinden, C.A., Dammers, E., Fogal, A., 2024. Biomass burning CO emissions: exploring insights through TROPOMI-derived emissions and emission coefficients. Atmospheric Chemistry and Physics 24, 10159–10186. https://doi.org/10.5194/acp-24-10159-2024

Guo, M., Fang, S., Liu, S., Liang, M., Wu, H., Yang, L., Li, Z., Liu, P., Zhang, F., 2020. Comparison of Atmospheric CO2, CH4, and CO at Two Stations in the Tibetan Plateau of China. Earth and Space Science 7, e2019EA001051. https://doi.org/10.1029/2019EA001051

Hase, F., Frey, M., Blumenstock, T., Groß, J., Kiel, M., Kohlhepp, R., Mengistu Tsidu, G., Schäfer, K., Sha, M.K., Orphal, J., 2015. Application of portable FTIR spectrometers for detecting greenhouse gas emissions of the major city Berlin. Atmos. Meas. Tech. 8, 3059–3068. https://doi.org/10.5194/amt-8-3059-2015

Hase, F., Frey, M., Kiel, M., Blumenstock, T., Harig, R., Keens, A., Orphal, J., 2016. Addition of a channel for XCO observations to a portable FTIR spectrometer for greenhouse gas measurements. Atmos. Meas. Tech. 9, 2303–2313. https://doi.org/10.5194/amt-9-2303-2016

Hasekamp, O.P., Butz, A., 2008. Efficient calculation of intensity and polarization spectra in vertically inhomogeneous scattering and absorbing atmospheres. Journal of Geophysical Research: Atmospheres 113. https://doi.org/10.1029/2008JD010379

Herkommer, B., Alberti, C., Castracane, P., Chen, J., Dehn, A., Dietrich, F., Deutscher, N.M., Frey, M.M., Groß, J., Gillespie, L., Hase, F., Morino, I., Pak, N.M., Walker, B., Wunch, D., 2024. Using a portable FTIR spectrometer to evaluate the consistency of Total Carbon Column Observing Network (TCCON) measurements on a global scale: the Collaborative Carbon Column Observing Network (COCCON) travel standard. Atmospheric Measurement Techniques 17, 3467–3494. https://doi.org/10.5194/amt-17-3467-2024

Hurtmans, D., Coheur, P.-F., Wespes, C., Clarisse, L., Scharf, O., Clerbaux, C., Hadji-Lazaro, J., George, M., Turquety, S., 2012. FORLI radiative transfer and retrieval code for IASI. Journal of Quantitative Spectroscopy and

https://doi.org/10.5194/egusphere-2025-966
Preprint. Discussion started: 1 April 2025

Radiative Transfer, Three Leaders in Spectroscopy 113, 1391–1408. https://doi.org/10.1016/j.jqsrt.2012.02.036

Kang, Y., Choi, H., Im, J., Park, S., Shin, M., Song, C.-K., Kim, S., 2021. Estimation of surface-level NO2 and O3 concentrations using TROPOMI data and machine learning over East Asia. Environmental Pollution 288, 117711. https://doi.org/10.1016/j.envpol.2021.117711

Landgraf, J., aan de Brugh, J., Scheepmaker, R., Borsdorff, T., Hu, H., Houweling, S., Butz, A., Aben, I., Hasekamp, O., 2016. Carbon monoxide total column retrievals from TROPOMI shortwave infrared measurements. Atmospheric Measurement Techniques 9, 4955–4975. https://doi.org/10.5194/amt-9-4955-2016

Lee, J., Jeong, S., Park, H., Hong, J., Kim, J., Frey, M.M., Morino, I., Ohyama, H., Hase, F., Mermigkas, M., Zhou, M., Té, Y., Roehl, C.M., 2024. Emission Characteristics of Greenhouse Gases and Air Pollutants in Northern Hemisphere Cities: Comprehensive Assessment Using Ground-Based Fourier Transform Spectrometers. Journal of Geophysical Research: Atmospheres 129, e2023JD040562. https://doi.org/10.1029/2023JD040562

Luther, A., Kleinschek, R., Scheidweiler, L., Defratyka, S., Stanisavljevic, M., Forstmaier, A., Dandocsi, A., Wolff, S., Dubravica, D., Wildmann, N., Kostinek, J., Jöckel, P., Nickl, A.-L., Klausner, T., Hase, F., Frey, M., Chen, J., Dietrich, F., Nęcki, J., Swolkień, J., Fix, A., Roiger, A., Butz, A., 2019. Quantifying CH_4 emissions from hard coal mines using mobile sun-viewing Fourier transform spectrometry. Atmospheric Measurement Techniques 12, 5217–5230. https://doi.org/10.5194/amt-12-5217-2019

Methodology and applications of city level CO2 emission accounts in China, 2017. . Journal of Cleaner Production 161, 1215–1225. https://doi.org/10.1016/j.jclepro.2017.06.075

Shan, Y., Guan, D., Hubacek, K., Zheng, B., Davis, S.J., Jia, L., Liu, J., Liu, Z., Fromer, N., Mi, Z., Meng, J., Deng, X., Li, Y., Lin, J., Schroeder, H., Weisz, H., Schellnhuber, H.J., 2018. City-level climate change mitigation in China. Science Advances 4, eaaq0390. https://doi.org/10.1126/sciadv.aaq0390

Sim, S., Jeong, S., Park, H., Park, C., Kwak, K.-H., Lee, S.-B., Kim, C.H., Lee, S., Chang, J.S., Kang, H., Woo, J.-H., 2020. Co-benefit potential of urban CO2 and air quality monitoring: A study on the first mobile campaign and building monitoring experiments in Seoul during the winter. Atmospheric Pollution Research 11, 1963–1970. https://doi.org/10.1016/j.apr.2020.08.009

Soulie, A., Granier, C., Darras, S., Zilbermann, N., Doumbia, T., Guevara, M., Jalkanen, J.-P., Keita, S., Liousse, C., Crippa, M., Guizzardi, D., Hoesly, R., Smith, S.J., 2024. Global anthropogenic emissions (CAMS-GLOB-ANT) for the Copernicus Atmosphere Monitoring Service simulations of air quality forecasts and reanalyses. Earth System Science Data 16, 2261–2279. https://doi.org/10.5194/essd-16-2261-2024

Spivakovsky, C.M., Logan, J.A., Montzka, S.A., Balkanski, Y.J., Foreman-Fowler, M., Jones, D.B.A., Horowitz, L.W., Fusco, A.C., Brenninkmeijer, C. a. M., Prather, M.J., Wofsy, S.C., McElroy, M.B., 2000. Three-dimensional

https://doi.org/10.5194/egusphere-2025-966
Preprint. Discussion started: 1 April 2025

climatological distribution of tropospheric OH: Update and evaluation. Journal of Geophysical Research: Atmospheres 105, 8931–8980. https://doi.org/10.1029/1999JD901006

Thompson, A.M., 1992. The Oxidizing Capacity of the Earth's Atmosphere: Probable Past and Future Changes | Science [WWW Document]. URL https://www.science.org/doi/10.1126/science.256.5060.1157 (accessed 12.29.24).

Tu, Q., Hase, F., Blumenstock, T., Kivi, R., Heikkinen, P., Sha, M.K., Raffalski, U., Landgraf, J., Lorente, A., Borsdorff, T., Chen, H., Dietrich, F., Chen, J., 2020. Intercomparison of atmospheric CO_2 and CH_4 abundances on regional scales in boreal areas using Copernicus Atmosphere Monitoring Service (CAMS) analysis, COllaborative Carbon Column Observing Network (COCCON) spectrometers, and Sentinel-5 Precursor satellite observations. Atmospheric Measurement Techniques 13, 4751–4771. https://doi.org/10.5194/amt-13-4751-2020

Tu, Q., Hase, F., Blumenstock, T., Schneider, M., Schneider, A., Kivi, R., Heikkinen, P., Ertl, B., Diekmann, C., Khosrawi, F., Sommer, M., Borsdorff, T., Raffalski, U., 2021. Intercomparison of arctic XH_2O observations from three ground-based Fourier transform infrared networks and application for satellite validation. Atmospheric Measurement Techniques 14, 1993–2011. https://doi.org/10.5194/amt-14-1993-2021

Tu, Q., Hase, F., Chen, Z., Schneider, M., García, O., Khosrawi, F., Chen, S., Blumenstock, T., Liu, F., Qin, K., Cohen, J., He, Q., Lin, S., Jiang, H., Fang, D., 2023. Estimation of NO_2 emission strengths over Riyadh and Madrid from space from a combination of wind-assigned anomalies and a machine learning technique. Atmospheric Measurement Techniques 16, 2237–2262. https://doi.org/10.5194/amt-16-2237-2023

Tu, Q., Hase, F., Qin, K., Alberti, C., Lu, F., Bian, Z., Cao, L., Fang, J., Gu, J., Guan, L., Jiang, Y., Kang, H., Liu, W., Liu, Y., Lu, L., Shan, Y., Si, Y., Xu, Q., Ye, C., 2024a. COCCON Measurements of XCO2, XCH4 and XCO over Coal Mine Aggregation Areas in Shanxi, China, and Comparison to TROPOMI and CAMS Datasets. Remote Sensing 16, 4022. https://doi.org/10.3390/rs16214022

Tu, Q., Hase, F., Qin, K., Cohen, J.B., Khosrawi, F., Zou, X., Schneider, M., Lu, F., 2024b. Quantifying CH_4 emissions from coal mine aggregation areas in Shanxi, China, using TROPOMI observations and the wind-assigned anomaly method. Atmospheric Chemistry and Physics 24, 4875–4894. https://doi.org/10.5194/acp-24-4875-2024

Tu, Q., Hase, F., Schneider, M., García, O., Blumenstock, T., Borsdorff, T., Frey, M., Khosrawi, F., Lorente, A., Alberti, C., Bustos, J.J., Butz, A., Carreño, V., Cuevas, E., Curcoll, R., Diekmann, C.J., Dubravica, D., Ertl, B., Estruch, C., León-Luis, S.F., Marrero, C., Morgui, J.-A., Ramos, R., Scharun, C., Schneider, C., Sepúlveda, E., Toledano, C., Torres, C., 2022a. Quantification of CH_4 emissions from waste disposal sites near the city of Madrid using ground- and space-based observations of COCCON, TROPOMI and IASI. Atmospheric Chemistry and Physics 22, 295–317. https://doi.org/10.5194/acp-22-295-2022

Tu, Q., Schneider, M., Hase, F., Khosrawi, F., Ertl, B., Necki, J., Dubravica, D., Diekmann, C.J., Blumenstock, T., Fang, D., 2022b. Quantifying CH_4 emissions in hard coal mines from TROPOMI and IASI observations

https://doi.org/10.5194/egusphere-2025-966
Preprint. Discussion started: 1 April 2025

using the wind-assigned anomaly method. Atmospheric Chemistry and Physics 22, 9747–9765. https://doi.org/10.5194/acp-22-9747-2022

Veefkind, J.P., Aben, I., McMullan, K., Förster, H., de Vries, J., Otter, G., Claas, J., Eskes, H.J., de Haan, J.F., Kleipool, Q., van Weele, M., Hasekamp, O., Hoogeveen, R., Landgraf, J., Snel, R., Tol, P., Ingmann, P., Voors, R., Kruizinga, B., Vink, R., Visser, H., Levelt, P.F., 2012. TROPOMI on the ESA Sentinel-5 Precursor: A GMES mission for global observations of the atmospheric composition for climate, air quality and ozone layer applications. Remote Sensing of Environment, The Sentinel Missions - New Opportunities for Science 120, 70–83. https://doi.org/10.1016/j.rse.2011.09.027

Wunch, D., Toon, G.C., Blavier, J.-F.L., Washenfelder, R.A., Notholt, J., Connor, B.J., Griffith, D.W.T., Sherlock, V., Wennberg, P.O., 2011. The Total Carbon Column Observing Network. Philosophical Transactions of the Royal Society A: Mathematical, Physical and Engineering Sciences 369, 2087–2112. https://doi.org/10.1098/rsta.2010.0240

Xiong, H., Lin, Y., Liu, S., Zang, K., Chen, Y., Liu, P., Liang, M., Jiang, K., Qing, X., Qiu, S., Hong, H., Li, J., Fang, S., 2022. Variations of atmospheric CO concentration from 2004 to 2019 at the Mt. Waliguan station in China. Atmospheric Research 271, 106060. https://doi.org/10.1016/j.atmosres.2022.106060

Zhang, G., Nan, Z., Hu, N., Yin, Z., Zhao, L., Cheng, G., Mu, C., 2022. Qinghai-Tibet Plateau Permafrost at Risk in the Late 21st Century. Earth's Future 10, e2022EF002652. https://doi.org/10.1029/2022EF002652

Zhou, M., Ni, Q., Cai, Z., Langerock, B., Jiang, J., Che, K., Wang, J., Nan, W., Liu, Y., Wang, P., 2023. Ground-Based Atmospheric CO2, CH4, and CO Column Measurements at Golmud in the Qinghai-Tibetan Plateau and Comparisons with TROPOMI/S5P Satellite Observations. Adv. Atmos. Sci. 40, 223–234. https://doi.org/10.1007/s00376-022-2116-0